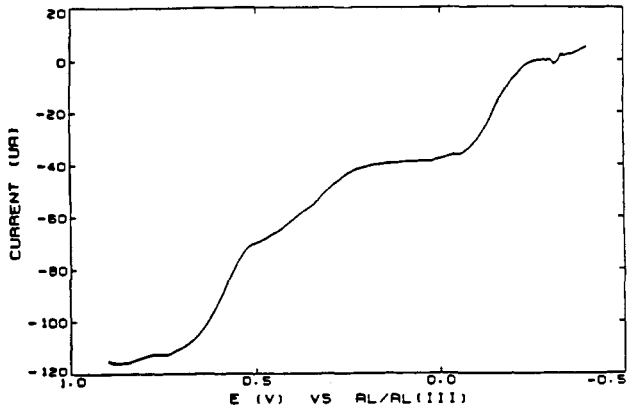


**Figure 2.** Normal-pulse voltammogram at Pt for oxidation of 16 mM $Mo_2Cl_8^{4-}$ ($t_p$ = 50 ms). Melt is basic $AlCl_3$–ImCl containing 0.4 M $EtAlCl_2$. Voltage is scanned from the open circuit potential in anodic direction.

in the presence of a large excess of $EtAlCl_2$.

The second one-electron-oxidation wave at the Pt electrode is relatively broad and shifts from 0.3 to 0.4 V as $\nu$ is increased from 10 to 500 mV/s. Also, at the higher scan rates, the ratio $I_p^a/\nu^{1/2}$ decreases. These observations are indicative of an electrochemical process coupled with a homogeneous chemical reaction.[13] This is expected since the final product of the second oxidation has been shown to be $Mo_2Cl_9^{3-}$, the formation of which requires a degree of structural rearrangement of $Mo_2Cl_8^{4-}$.[1]

The $Mo_2Cl_8^{4-}$ oxidations were also examined by using normal-pulse voltammetry at the Pt electrode. Pulse widths, $t_p$, were varied from 50 to 1000 ms. After each analysis pulse, the melt was stirred for 2 s and then left unstirred for 5 s before applying the next more anodic pulse. A normal-pulse voltammogram is shown in Figure 2. Three distinct waves are apparent corresponding to first, a one-electron oxidation of $Mo_2Cl_8^{4-}$ to $Mo_2Cl_8^{3-}$, second, a one-electron oxidation of $Mo_2Cl_8^{3-}$ to $Mo_2Cl_9^{3-}$, and finally, a one-electron oxidation of $Mo_2Cl_9^{3-}$ to $Mo_2Cl_9^{2-}$. The position and shapes of the first and third oxidation waves remained essentially invariant with changing pulse width as expected for reversible processes.[14] The limiting current plateau, $i_{lim}$, for the second oxidation, however, was not easily discernible especially at the shorter pulse widths. Despite the less than ideal second wave, the ratios of limiting currents for the three oxidations were approximately 1:1:1 as expected for electrochemical processes under diffusion control. A plot of $i_{lim}$ vs. $t_p^{1/2}$ for the first oxidation wave is linear and passes through the origin. From the slope of this plot, a $D$ value of $(2.61 \pm 0.03) \times 10^{-7}$ cm$^2$/s for $Mo_2Cl_8^{4-}$ was calculated.[15] This value is consistent with previously determined dimer diffusion coefficients.[1]

## Conclusions

In the acidic $AlCl_3$–ImCl molten salt, the molybdenum dimers, $Mo_2Cl_8^{4-}$ and $Mo_2Cl_8H^{3-}$, are easily interconverted by using $ImHCl_2$ as a proton source and $EtAlCl_2$ as a proton-removing reagent. The presence of excess $EtAlCl_2$ in the melt does not alter the electrochemistry of $Mo_2Cl_8^{4-}$. These two reagents should prove useful in examining the interaction of hydrogen with other metal clusters in these unique solvent systems.

**Acknowledgment.** This work was supported in part by the Office of Naval Research and the Air Force Office of Scientific Research.

**Registry No.** $Mo_2(OAc)_4$, 14221-06-8; $AlCl_3$, 7446-70-0; ImCl, 65039-09-0; $Mo_2Cl_8^{4-}$, 34767-26-5; $ImHCl_2$, 116210-73-2; $Mo_2Cl_8H^{3-}$, 66496-30-8; $EtAlCl_2$, 563-43-9; $Mo_2Cl_8^{3-}$, 64477-04-9; $Mo_2Cl_9^{3-}$, 52409-23-1; $Mo_2Cl_9^{2-}$, 51059-87-1.

(13) Greef, R.; Peat, R.; Peter, L. M.; Pletcher, D.; Robinson, J. *Instrumental Methods in Electrochemistry*; Kemp, T. J., Ed.; Ellis Horwood: Chichester, England, 1985, Chapter 6.
(14) Christie, J. H.; Parry, E. P.; Osteryoung, R. A. *Electrochim. Acta* **1966**, *11*, 1525.
(15) Parry, E. P.; Osteryoung, R. A. *Anal. Chem.* **1965**, *37*, 1654.

Contribution from the Centre d'Etudes Nucleaires de Grenoble, DRF-G/Service de Physique/Groupe SCPM, 85X 38041 Grenoble Cedex, France

# A Model for the Spin States of High-Potential $[Fe_4S_4]^{3+}$ Proteins

Louis Noodleman*

*Received March 8, 1988*

The complex and highly variable spin-state structures of $[Fe_3S_4]$ and $[Fe_4S_4]$ proteins and synthetic analogues are now well appreciated[1-4] but not well understood. Here, we propose and solve a simple Hamiltonian for the spin states of oxidized high-potential $[Fe_4S_4]^{3+}$ (HP) clusters. The relative energies of the low-lying spin states are analyzed including conditions for state crossings. We then use the vector model originally developed by Middleton[5] for reduced $[Fe_4S_4]^+$ and utilized by him also for $[Fe_4S_4]^{3+}$ to approximately evaluate effective isotropic $g$ and $A$ values. Important early experimental work on this system is due to Antanaitas and Moss.[5c] Middleton's vector model[5b] for $[Fe_4S_4]^{3+}$ is essentially correct, but one must also show how to generate the correct spin-state energies from the basic physics of the problem. Recent developments[4,6] in the spin coupling theory of mixed-valence antiferromagnetic (AF) complexes combined with quantitative calculations[7-9] make further progress possible.

To obtain the proper spin-state ordering for $[Fe_4S_4]^{3+}$ clusters requires at least two Heisenberg AF coupling parameters $J$ and also one resonance delocalization parameter $B$ for the mixed-valence pair $Fe^{3+}$–$Fe^{2+}$. In HP complexes, Mossbauer spectroscopy shows that four Fe sites occur in two internally equivalent pairs[1,5] designated $\beta$ for the $Fe^{3+}$–$Fe^{3+}$ and $\alpha$ for the $Fe^{3+}$–$Fe^{2+}$ mixed valence (equivalently $Fe^{2.5+}$). Quantitative X$\alpha$–VB calculations[7-9] on $[Fe_4S_4]^{3+,2+}$ models in $C_{2v}$ symmetry show that the electron undergoing delocalization resides in an orbital largely confined ($\geq$85%)[7b] to one $Fe_2S_2$ layer with bonding along the Fe–Fe axis. It appears, therefore, that one $B$ parameter confined to the mixed-valence pair is sufficient to describe resonance or double exchange in HP. The Heisenberg AF coupling constant should be largest in the $Fe^{3+}$–$Fe^{3+}$ pair and decrease in the order $Fe^{3+}$–$Fe^{3+}$ > $Fe^{3+}$–$Fe^{2.5+}$ > $Fe^{3+}$–$Fe^{2+}$; the second term represents an interlayer pair, and the third, the mixed-valence pair. (In the notation above, $Fe^{3+}$–$Fe^{2.5+}$ is used, since the relevant Heisenberg coupling links a ferric center with a mixed-valence center.) This order is verfied by our X$\alpha$–VB calculations on $[Fe_3S_4]^{+,0}$ clusters[8,9] and has been assumed in fitting $[Fe_4S_4]$ susceptibility data by others.[10]

The Mossbauer hyperfine structure of $[Fe_4S_4]^{3+}$ gives the surprising result that the effective $A$ values of the $Fe^{3+}$–$Fe^{3+}$ pair are positive,[1,9] so that the ferric pair spins are aligned oppositely to the net system spin $S = {}^1/_2$ in a magnetic field. (All $A$ values are with reference to the ground-state magnetic moment of the $^{57}$Fe nucleus.) Münck and Papaefthymiou[11] have proposed that $S_{12}' = 4$ is then required for the ferric pair spin. But how and why does this occur?

Consider a system spin Hamiltonian:

$$H = J(\vec{S}_1\cdot\vec{S}_2 + \vec{S}_1\cdot\vec{S}_3 + \vec{S}_1\cdot\vec{S}_4 + \vec{S}_2\cdot\vec{S}_3 + \vec{S}_2\cdot\vec{S}_4 + \vec{S}_3\cdot\vec{S}_4) \pm B(S_{34}' + {}^1/_2) + \Delta J_{12}(\vec{S}_1\cdot\vec{S}_2) + \Delta J_{34}(\vec{S}_3\cdot\vec{S}_4) \quad (1)$$

$S_1$ and $S_2$ are site spins for $Fe^{3+}$–$Fe^{3+}$, and $S_3$ and $S_4$, site spins for $Fe^{3+}$–$Fe^{2+}$, so $S_1 = S_2 = {}^5/_2$, $S_3 = {}^5/_2$, and $S_4 = 2$. (The last two spin values can be interchanged without affecting the argument.) The interlayer coupling constant linking one site of pair $\alpha$ with one site of pair $\beta$ is $J$ describing four equal interlayer site couplings, while the ferric ($\beta$) pair and mixed-valence ($\alpha$) pair couplings are $J_{12} = J + \Delta J_{12}$ and $J_{34} = J + \Delta J_{34}$, respectively. In a more general context, the $B$ resonance term can be derived

* Address correspondence to Department of Molecular Biology MB1, Research Institute of Scripps Clinic, La Jolla, CA 92037.

0020-1669/88/1327-3677$01.50/0 

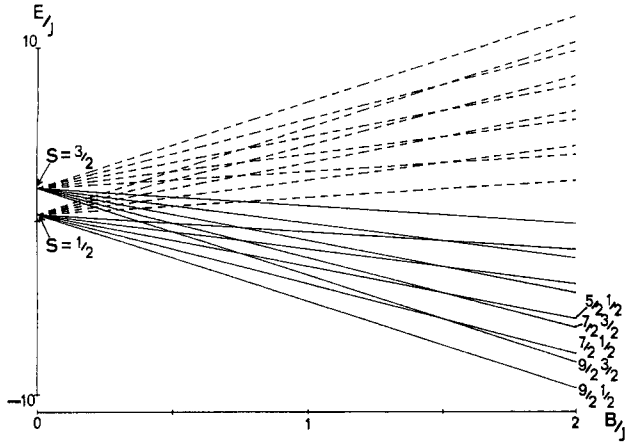


**Figure 1.** Plot of $E/J$ vs $B/J$ for $S = {}^1/_2$ and ${}^3/_2$ at $\Delta J_{12} = \Delta J_{34} = 0$. The lower minus roots are represented by solid lines; the upper plus roots, by dashed lines.

from a transfer operator that generates the appropriate Racah coefficient.[4]

The general solution to this problem follows immediately, but it is useful to consider first the simpler case where all site AF couplings are $J$, so $\Delta J_{12} = 0$, $\Delta J_{34} = 0$, and the state energies are[4]

$$E(S_{34}',S) = (J/2)[S(S+1)] \bullet B(S_{34}' + {}^1/_2) \qquad (2)$$

with the pair spin vectors $\vec{S}_{12}'$ and $\vec{S}_{34}'$. The detailed states are enumerated via the triangle inequality.[12] $S_{12}'$ has the unrestricted range $0 \le S_{12}' \le 5$; for $S_{34}'$, ${}^1/_2 \le S_{34}' \le {}^9/_2$. Since $\vec{S}_{12}' + \vec{S}_{34}' = \vec{S}$, the corresponding quantum numbers also obey triangle inequalities. For specific $S$ and $S_{34}'$, the $S_{12}'$ values are also restricted to

$$(S + S_{34}') \ge S_{12}' \ge |S - S_{34}'| \qquad (3)$$

This relation is symmetric in the three spin vectors, so the range of each is similarly restricted; for example, $(S_{12}' + S_{34}') \ge S \ge |S_{12}' - S_{34}'|$. Equations 2 and 3 demonstrate that, for equal $J$ values, the states are degenerate in $S_{12}'$. In Figure 1, we give a plot of eq 2 for some of the low-lying spin states $|S_{34}'\ S\rangle_{+,-}$. As the minus roots of eq 2 are always lower than the plus roots for positive $B$, we will focus on these. For all $J$'s equal, $|{}^9/_2\ {}^1/_2\rangle_-$ is the ground state for the whole range of $B/J$ when $J$ is positive (AF) This is in contrast to the analogous reduced $[Fe_3S_4]^0$ ground state where the mixed-valence dimer spin $S_{AB}$ and total spin $S$ change as a function of $B/J$.[4] However, the physically important case includes $\Delta J_{12} \neq 0$.

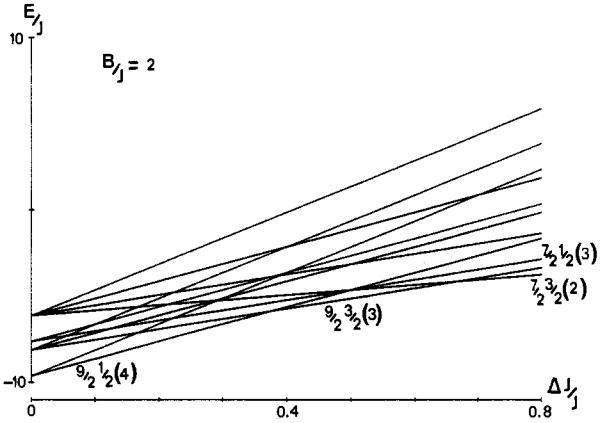


**Figure 2.** The four lowest states in Figure 1 plotted at $B/J = 2$ for $\Delta J_{12}/J > 0$ and $\Delta J_{34} = 0$. This plane perpendicular to that in Figure 1, and $\Delta J$ is $\Delta J_{12}$.

The general solution to eq 1 is

$$E(S_{34}',S,S_{12}') = (J/2)[S(S+1)] \pm B(S_{34}' + {}^1/_2) + (\Delta J_{12}/2)[S_{12}'(S_{12}'+1)] + (\Delta J_{34}/2)[S_{34}'(S_{34}'+1)] \qquad (4)$$

Our notation for complete spin states is $[S_{34}'\ S\ (S_{12}')\rangle$. With all $J$'s equal, the ground $|{}^9/_2\ {}^1/_2\rangle_-$ is degenerate with $S_{12}' = 4$ and 5 as the sublevels. The $\Delta J_{12}$ perturbation is positive since $J(Fe^{3+}\text{-}Fe^{3+})$ is the strongest AF coupling parameter, so $|{}^9/_2\ {}^1/_2\ (4)\rangle$ is always lower in energy than $|{}^9/_2\ {}^1/_2\ (5)\rangle_-$ by $5\Delta J_{12}$. We have, therefore, predicted by energetic considerations alone the correct $|{}^9/_2\ {}^1/_2\ (4)\rangle$ substate necessary to explain the Mössbauer A tensor data. According to the present scheme, the lowest excited state is $|{}^9/_2\ {}^3/_2\ (3)\rangle$ since for $|{}^9/_2\ {}^3/_2\rangle$ the sublevels $S_{12}' = 3$, 4, 5 are possible. This state is found at $\Delta E = {}^3/_2 J - 4\Delta J_{12}$ above $|{}^9/_2\ {}^1/_2\ (4)\rangle$, as seen in Figure 2. A state crossing is found at $\Delta J/J = {}^3/_8$ with $|{}^9/_2\ {}^3/_2\ (3)\rangle$ the ground state for larger $\Delta J/J$. Our calculations on oxidized and reduced $[Fe_3S_4]^{+,0}$ clusters[8,9] give a typical $\Delta J/J$ of about 0.25 and $B/J \ge 1.4$, which is within the expected range for a $|{}^9/_2\ {}^1/_2\ (4)\rangle$ ground state in HP. Since the lowest $S = {}^3/_2$ excited state would be of considerable interest for ESR, NMR, and magnetic susceptibility measurements, we will estimate its position. For a typical $Fe^{3+}$ pair $J_{12}$ value of $J + \Delta J = 450\ cm^{-1}$ and $\Delta J = 90\ cm^{-1}$, we find $\Delta E = 180\ cm^{-1}$ approximately, which may be observable. Also, $|{}^9/_2\ {}^1/_2\ (5)\rangle$ would lie at about $5\Delta J = 450\ cm^{-1}$. This would be difficult to observe unless $\Delta J$ were much smaller. All other state energies are calculable from eq 4. If the $\Delta J_{34}$ term for the mixed-valence pair is negative, this simply reinforces the $S_{34}' = {}^9/_2$ stability, the effect being the same on all states with the same $S_{34}'$. The most interesting phenomena occur when $B$ is drastically reduced. Then modest changes in $\Delta J_{12}$ and $\Delta J_{34}$ can lead to radically different spin-state orderings. This apparently happens in certain forms of reduced $[Fe_4Se_4]^+$ and $[Fe_4S_4]^+$ clusters.[1-3] The normal $|{}^9/_2\ {}^1/_2\ (4)\rangle$ ground state is replaced by those with $S = {}^3/_2$ or ${}^7/_2$ and the parallel alignment of spins in the mixed-valence pair is destroyed;[1-3] see eq 4 and Figure 1 for small $B/J$. In HP complexes, however, $B$ is evidently large, probably of the order of 500 $cm^{-1}$, as we have calculated in $[Fe_2S_2]^+$ and $[Fe_3S_4]^0$ clusters.[7-9] Quantitative calculations on HP models are currently in progress.

**Vector Model for g and A Tensors.** With assignment of all the spin quantum numbers, the vector model can be used as a consequence of the Wigner–Eckart theorem. Middleton et al. applied this method quantitatively to reduced $[Fe_4S_4]^+$ centers[5a] and qualitatively to high-potential $[Fe_4S_4]^{3+}$.[5b] The observed effective $A_i$ are related to the intrinsic site hyperfine $a_i$ by[4]

$$A_i = a_i \frac{\langle S_{iz} \rangle}{\langle S_z \rangle} = K_i a_i \qquad (5)$$

while for $g_{eff}$


(1) Papaefthymiou, V.; Millar, M. M.; Münck, E. *Inorg. Chem.* **1986**, *25*, 3010.
(2) Moulis, J. M.; Auric, P.; Gaillard, J.; Meyer, J. *J. Biol. Chem.* **1984**, *259*, 11396. Gaillard, J.; Moulis, J. M.; Auric, P.; Meyer, J. *Biochemistry* **1986**, *25*, 464.
(3) Lindahl, P. A.; Day, E. P.; Kent, T. A.; Orme-Johnson, W. H.; Münck, E. *J. Biol. Chem.* **1985**, *260*, 11160.
(4) Papaefthymiou, V.; Girerd, J. J.; Moura, I.; Moura, J. J. G.; Münck, E. *J. Am. Chem. Soc.* **1987**, *109*, 4703. Münck, E.; Papaefthymiou, V.; Surerus, K. K.; Girerd, J. J. In *Metals in Proteins*; ACS Symposium Series; Que, L., Ed.; American Chemical Society: Washington, DC, 1988.
(5) (a) Middleton, P.; Dickson, D. P. E.; Johnson, C. E.; Rush, J. D. *Eur. J. Biochem.* **1978**, *88*, 135. (b) *Ibid.* **1980**, *104*, 289. (c) Antanaitas, B. C.; Moss, T. H. *Biochim. Biophys. Acta* **1975**, *405*, 262.
(6) Belinskii, M. I. *Mol. Phys.* **1987**, *60*, 793.
(7) (a) Noodleman, L.; Baerends, E. J. *J. Am. Chem. Soc.* **1984**, *106*, 2316. (b) Noodleman, L.; Norman, J. G., Jr.; Osborne, J. H.; Aizman, A.; Case, D. A. *J. Am. Chem. Soc.* **1985**, *107*, 3418.
(8) Sontum, S. F.; Noodleman, L.; Case, D. A. In *Computational Chemistry: The Challenge of d and f Electrons*; ACS Symposium Series; Salahub, D. R., Zerner, M., Eds.; American Chemical Society: Washington, DC, 1988.
(9) Noodleman, L.; Case, D. A.; Aizman, A. *J. Am. Chem. Soc.* **1988**, *110*, 1001.
(10) Papaefthymiou, G. C.; Laskowski, E. J.; Frota-Pessoa, S.; Frankel, R. B.; Holm, R. H. *Inorg. Chem.* **1982**, *21*, 1723.
(11) Münck, E.; Papaefthymiou, V., personal communication.
(12) Brink, D. M.; Satchler, G. R. *Angular Momentum*, 2nd ed.; Oxford University Press: London, 1968.

$$g_{\text{eff}} = \sum_i K_i g_i \qquad (6)$$

Successive application of the Wigner–Eckart theorem to the site spins and pair spins gives

$$K_1 = K_2 = \frac{\langle S_{1z}\rangle}{\langle S_z\rangle} = \frac{\alpha\gamma}{\Delta_1} \qquad (7)$$

$$K_3 = \frac{\langle S_{3z}\rangle}{\langle S_z\rangle} = \frac{\delta_1\epsilon}{\Delta_2} \qquad K_4 = \frac{\langle S_{4z}\rangle}{\langle S_z\rangle} = \frac{\delta_2\epsilon}{\Delta_2} \qquad (8)$$

where

$$\alpha = [S_{12}'(S_{12}'+1) + S_1(S_1+1) - S_2(S_2+1)]/2$$
$$\gamma = [S(S+1) + S_{12}'(S_{12}'+1) - S_{34}'(S_{34}'+1)]/2$$
$$\Delta_1 = S_{12}'(S_{12}'+1)S(S+1)$$
$$\epsilon = [S(S+1) + S_{34}'(S_{34}'+1) - S_{12}'(S_{12}'+1)]/2$$
$$\delta_1 = [S_{34}'(S_{34}'+1) + S_3(S_3+1) - S_4(S_4+1)]/2$$
$$\delta_2 = [S_{34}'(S_{34}'+1) + S_4(S_4+1) - S_3(S_3+1)]/2$$
$$\Delta_2 = S_{34}'(S_{34}'+1)S(S+1) \qquad (9)$$

Since the sites 3 and 4 form a mixed-valence pair, it is necessary to average $A_3$ and $A_4$ for these sites. (We assume $S_3 = {}^5/_2$ and $S_4 = 2$ as a convention.) Site a values for typical monomeric compounds are $a(Fe^{3+}) = -20$ MHz and $a(Fe^{2+}) = -22$ MHz,[4] so that for HP in the ground $|{}^9/_2\ {}^1/_2\ (4)\rangle$ state we predict $K_1 = -{}^4/_3$, $K_3 = {}^{55}/_{27}$, $K_4 = {}^{44}/_{27}$, and

$$A_1 = A_2 = +26.7 \text{ MHz}$$
$$A_{3,4}^{\text{av}} = -38.5 \text{ MHz} \qquad (10)$$

compared with $A_1 = +20.2$ and $A_{3,4}^{\text{av}} = -32.0$ MHz experimentally. For the excited substate $|{}^9/_2\ {}^1/_2\ (5)\rangle$, we predict $A_1 = A_2 = -40$ MHz and $A_{3,4}^{\text{av}} = +31.3$ MHz, in contrast to experiment. For the excited $|{}^9/_2\ {}^3/_2\ (3)\rangle$ state, we find $A_1 = +12$ MHz and $A_{3,4}^{\text{av}} = -23$ MHz, which can be compared with the observed hyperfine coupling only after the $S = {}^3/_2$ state is identified and its hyperfine coupling obtained by ENDOR or magnetic Mössbauer spectroscopy. This is not presently available.

If there were three local ${}^5/_2$ spins and one local $S_4 = 2$ spin with $g(Fe^{3+}) = 2.002$ and $g_4(Fe^{2+}) = 2.002 + \Delta g_4$, then $g_{\text{eff}} = 2.002 + {}^{44}/_{27}\Delta g_4$. With a ferrous $\Delta g_4^{\text{av}} = 0.05$ (see ref 7a), we calculate $g_{\text{eff}}^{\text{av}} = 2.08$, in good agreement with typical HP $g_{\text{av}} = 2.06$. However, the $S_3$–$S_4$ pair is totally delocalized, so it is better to calculate $\Delta g_{34}$ for the complete $S_{34}' = {}^9/_2$ subdimer.

Detailed quantitative calculations on HP models are under way and experiments are planned to more thoroughly explore this theoretical model.

**Acknowledgment.** I am grateful for discussions with J. Gaillard, E. Munck, E. P. Day, G. Ruis, B. Lamotte, J. Jordanov, J. M. Moulis, and D. Case. J. Gaillard also helped to construct the figures. This research was financially supported by the CENG.

---

Contribution from the Department of Chemistry,
California State University, Los Angeles,
Los Angeles, California 90032

## Conversion of *closo*-2,4-$C_2B_5H_7$ to [*nido*-2,4-$C_2B_4H_7$]$^-$

Zahid J. Abdou, Frank Gomez, Gaby Abdou,
and Thomas Onak*

*Received February 3, 1988*

The [*nido*-2,4-$C_2B_4H_7$]$^-$ ion has been previously prepared from a cage-opening reaction of *closo*-1,6-$C_2B_4H_6$ with metal hydrides or from the treatment of 5-$(CH_3)_3$N-*nido*-2,4-$C_2B_4H_6$ with a metal hydride.[1,2] Both reactions are very slow and, of course, depend upon the availability of *closo*-1,6-$C_2B_4H_6$. One of the most accessible small carboranes[3-5] is *closo*-2,4-$C_2B_5H_7$, and thus it became desirable to find a method for the removal of a boron from this $C_2B_5$ cage compound with the prospect of finding another route to the [*nido*-2,4-$C_2B_4H_7$]$^-$ ion.

### Experimental Section

**Materials and Handling of Chemicals.** The parent *closo*-carborane 2,4-$C_2B_5H_7$ was obtained from R. E. Williams and used without further purification. Standard high-vacuum techniques were used in the handling of all chemicals.

**Instrumentation.** Proton (400- and 500-MHz) spectra were obtained by use of Bruker AM and Bruker WM instruments, respectively. All $^{11}$B NMR chemical shift data are based on $\delta(BF_3{\cdot}OEt_2) = 0.00$ with negative values upfield.

**Reaction of *closo*-2,4-$C_2B_5H_7$ with Lithium Amides. (a) With Li[$N(CH_3)_2$].** To a 3-mm NMR tube, equipped at one end with a 2.5-mL bulb, was added Li[$N(CH_3)_2$] (Aldrich, 0.19 mmol) under a nitrogen atmosphere. After the tube and its contents were attached to a high-vacuum apparatus, *closo*-2,4-$C_2B_5H_7$ (0.13 mmol) was condensed into the tube at −195 °C. The mixture was subsequently warmed to room temperature, mixed well by shaking the sample, and then allowed to stand for approximately 2 min. After the sample was cooled back to −195 °C, $CH_3CN$ (Wilmad, 2 mmol) was added and the tube sealed and warmed to ambient temperature. The sample slowly turned to a clear yellow liquid, with no solids present. After the sample was kept at room temperature for 5.5 h, a $^{11}$B NMR spectrum indicated the presence of (a) [*nido*-2,4-$C_2B_4H_7$]$^-$ (2%) ($^{11}$B NMR: $\delta$(B(1)) −52.0, $J$(BH) = 158 Hz; $\delta$(B(3)) +21.3, $J$(BH) = 121 Hz; $\delta$(B(5,6)) +1.2, $J$(BH) = 133 Hz),[1,2] (b) starting material, *closo*-2,4-$C_2B_5H_7$[6] (97%), and traces of other compounds. After 28 h at ambient temperature the quantity of [2,4-$C_2B_4H_7$]$^-$ increased to 10% at the expense of the $C_2B_5H_7$. After 12 days at room temperature, four boron-containing cage compounds were evident: $C_2B_5H_7$ (48%), [2,4-$C_2B_4H_7$]$^-$ (29%), compound A (6%) $^{11}$B NMR: $\delta$ −39.1 (d), $J$(BH) = 153 Hz; $\delta$ +7 (d); $\delta$ +21 (d); $\delta$ +49 (d)), and compound B (7%) (high-field B(1) resonance at $\delta$ −50), and approximately 10% of other boron-containing species with an assortment of resonances appearing in the regions of $\delta$ +28, +15, −5, −10 to −20, and −44. One month later the percentage of [2,4-$C_2B_4H_7$]$^-$ climbed to 76%, and after 2 months 95% of all of the boron content was attributed to this ion with the remaining $^{11}$B resonances found at $\delta$ −7 and −15 to −25; no evidence of the starting material $C_2B_5H_7$, nor of compounds A and B, was found.

**(b) With Li[$N(C_2H_5)_2$].** In a manner similar to that described in section a Li[$N(C_2H_5)_2$] (Aldrich, 0.195 mmol), *closo*-2,4-$C_2B_5H_7$ (0.195 mmol), and $CD_3CN$ (2 mmol) were mixed. After 1 day at ambient temperature the clear liquid sample was yellow with no solids present. NMR data revealed the presence of (a) [*nido*-2,4-$C_2B_4H_7$]$^-$ (39%) ($^{11}$B NMR: $\delta$(B(1)) −52.9, $J$(BH) = 158 Hz; $\delta$(B(3)) +20.7, $J$(BH) = 119 Hz; $\delta$(B(5,6)) +0.4, $J$(BH) = 136 Hz. $^1$H NMR: $\delta$(H(1)) −1.59, $J$(HB) = 157 Hz; $\delta$((H$\mu$)) −4.57 (broad)),[1,2] (b) starting material, *closo*-2,4-$C_2B_5H_7$[6] (45%), and small amounts of compounds A (11%) and B (5%). $^{11}$B NMR data for A: $\delta$ −39.1 (area 1), $J$(BH) = 154 Hz; $\delta$ +6.7 (area 2), $J$(BH) = 131 Hz; $\delta$ +21.0 (area 1), $J$(BH) = ca. 118 Hz; $\delta$ +48.5 (area 1) (half-width ca. 260 Hz, which narrows to 170 Hz upon proton decoupling). $^{11}$B NMR data for compound B: $\delta$ −48.1 (area 1), $J$(BH) = 151 Hz; $\delta$ ca. −21 (area 2), $J$(BH) = 176 Hz; $\delta$ +20.7 (doublet, area 1). After the mixture was left to stand at room temperature for an additional 6 days, the $^{11}$B NMR spectrum of the sample exhibited the same resonances as observed before, but with slightly different intensities, leading to the following composition assessment: [*nido*-2,4-$C_2B_4H_7$]$^-$, 37%; *closo*-2,4-$C_2B_5H_7$, 49%; A, 7%; B, 7%. After 1 month at room temperature nearly equal amounts of the starting material, *closo*-2,4-$C_2B_5H_7$, and [*nido*-2,4-$C_2B_4H_7$]$^-$ were present, as assessed by the $^{11}$B NMR pattern. No further change occurred with time.

In another experiment with $C_2B_5H_7$/Li[$N(C_2H_5)_2$] (0.25 and 0.17 mmol, respectively) dissolved in 1.5 mmol of deuteriated acetonitrile, the

(1) Lockman, B.; Onak, T. *J. Am. Chem. Soc.* **1972**, *94*, 7923–7924.
(2) Onak, T.; Lockman, B.; Haran, G. *J. Chem. Soc., Dalton Trans.* **1973**, 2115–2118.
(3) Grimes, R. N. *Carboranes*; Academic: New York, 1970. Williams, R. E. *Adv. Inorg. Chem. Radiochem.* **1976**, *18*, 67–142.
(4) Onak, T. Polyhedral Organoboranes. In *Comprehensive Organometallic Chemistry*; Pergamon: Oxford, England, 1982; pp 411–457.
(5) Onak, T. Carboranes. In *Gmelin Handbook of Inorganic Chemistry*; Springer-Verlag: Berlin, FRG, 1981; Boron Compounds 1st Suppl. Vol. 3, pp 105–256; *Ibid.* Springer-Verlag: Berlin, FRG, 1982; Boron Compounds 2nd Suppl. Vol. 2, pp 223–335.
(6) Eaton, G. R.; Lipscomb, W. N. *NMR Studies of Boron Hydrides and Related Compounds*; Benjamin: New York, 1969.

0020-1669/88/1327-3679$01.50/0 